APS physics

CHORUS

This is the accepted manuscript made available via CHORUS. The article has been published as:

Theoretical study of the spin and charge dynamics of two-leg ladders as probed by resonant inelastic x-ray scattering

Umesh Kumar, Alberto Nocera, Elbio Dagotto, and Steven Johnston

Phys. Rev. B **99**, 205130 — Published 17 May 2019

DOI: 10.1103/PhysRevB.99.205130

Theoretical study of the spin and charge dynamics of two-leg ladders as probed by resonant inelastic x-ray scattering

Umesh Kumar,[1,2] Alberto Nocera,[1,3,4] Elbio Dagotto,[1,3] and Steven Johnston[1,2]

[1] *Department of Physics and Astronomy, The University of Tennessee, Knoxville, TN 37996, USA*
[2] *Joint Institute for Advanced Materials, The University of Tennessee, Knoxville, TN 37996, USA*
[3] *Materials Science and Technology Division, Oak Ridge National Laboratory, Oak Ridge, Tennessee 37831, USA*
[4] *Stewart Blusson Quantum Matter Institute, University of British Columbia, Vancouver, British Columbia V6T 1Z4, Canada*

(Dated: May 6, 2019)

Resonant inelastic x-ray scattering (RIXS) has become an important tool for studying elementary excitations in correlated materials. Here, we present a systematic theoretical investigation of the Cu L-edge RIXS spectra of undoped and doped cuprate two-leg spin-ladders in both the non-spin-conserving (NSC) and spin-conserving (SC) channels. The spectra are rich and host many exotic excitations. In the NSC-channel of the undoped case, we identify one-triplon and bound *triplet* two-triplon excitations in the strong-rung coupling limit, as well as confined spinons in the weak-rung coupling limit. In the doped case, we observe a quasiparticle excitation formed from a bound charge and spin-$\frac{1}{2}$ in the strong-rung coupling limit. In the SC-channel, we also identify several new features, including bound *singlet* two-triplon excitations and confined spinons in the undoped ladders in the strong- and weak-rung coupling limits, respectively. Conversely, in the doped case, the SC channel primarily probes both gapless and gapped charge excitations. Finally, we revisit the available data for the ladder compound $Sr_{14}Cu_{24}O_{41}$ in the context of our results.

I. INTRODUCTION

Strongly correlated spin ladders are excellent platforms for studying quantum many-body phenomena, such as high critical temperature (high-T_c) superconductivity [1] and spinon confinement [2]. Quantum ladders are intermediate between one- and two-dimensional materials, and their study allows for detailed comparisons between theoretical models and experimental probes [2–20]. The discovery of superconductivity in the ladder "telephone number" compound $Sr_{0.4}Ca_{13.6}Cu_{24}O_{41.84}$ [21], which had been theoretically predicted [22], created new opportunities to study the relationships between lattice, orbital, charge, and magnetic degrees of freedom and unconventional superconductivity in copper-oxide materials. Accordingly, a significant effort has been launched to understand the magnetic excitation spectrum of materials hosting quantum ladders and its connection to superconductivity. For example, inelastic neutron scattering (INS) studies have reported the observation of a spin gap in $Sr_{14}Cu_{24}O_{41}$ [13], triplon and two-triplon excitations in $La_4Sr_{10}Cu_{24}O_{41}$ [23], and spinon confinement in $CaCu_2O_3$ [2].

With continued improvements in instrumentation, resonant inelastic x-ray scattering (RIXS) is being increasingly employed to study collective magnetic excitations [3–5, 24–30]. RIXS is complementary to INS in that the scattering processes allows for both $\Delta S = 0$ and $\Delta S = 1$ excitations, depending on the elemental edge [25, 31], the strength of the spin-orbit coupling in the core level [31], and the local crystal stucture of the material [32]. As such, the technique accesses many magnetic excitations including magnons [26–30] and bimagnons in two-dimensional (2D) cuprates [25, 33], and multi-spinon excitations in one-dimensional (1D) cuprates [4, 34–36]. RIXS also provided surprising results for 2D cuprates, where the paramagnon excitations are found to persist deep into the overdoped region of the phase diagram [26–29, 37]. Recently, an electron-hole asymmetry in the doping dependence of the spin excitations of 2D cuprates was reported, as well as an additional collective charge excitation in the electron-doped case that is absent in the hole-doped case [30].

The rich variety of excitations observed in 1D and 2D cuprates described above, and their possible connection to unconventional superconductivity, provides a strong motivation for exploring the RIXS spectra of two-leg spin ladders, both as a function of the rung coupling and doping. Such studies provide information not only about magnetic excitations but also about potentially cooperative/competing charge, orbital, and lattice excitations. Early RIXS Cu K-edge experiments on the telephone number compounds focused primarily on the high-energy charge excitations across the Mott gap [38–40]. Later, as the instrumental resolution improved, studies started addressing low-energy magnetic excitations. For example, the magnetic response of $Sr_{14}Cu_{24}O_{41}$ at the Cu L_3-edge was measured [5] and interpreted in terms of the lower boundaries of a two-triplon continuum. Another Cu L_3-edge study on $CaCu_2O_3$ – a weakly coupled spin-ladder system – showed that the spectra could be decomposed into contributions from the spin-conserving (SC) and non-spin-conserving (NSC) channels [41]. Subsequent work at the same edge on the same material focused on spin-orbital fractionalization, but did not carry out an analysis of spinon confinement [42].

From a theoretical perspective, studies of the RIXS response of spin ladders have mainly focused on undoped systems using a projector method [8] or exact diagonalization (ED) of small (4×2) Hubbard clusters [5], and were restricted to a limited set of rung couplings. To our knowledge, no systematic RIXS study of the low-energy

excitations of doped and undoped ladders has been carried out. Here, we present such a study. Specifically, we use the Kramers-Heisenberg formalism to compute the RIXS response of undoped and doped two-leg t-J ladders while varying the superexchange coupling along the rungs over a wide range of values. The RIXS intensity is evaluated numerically, exactly or with a very small error, using ED and the density matrix renormalization group (DMRG) [43–45] methods. Using these tools, we investigate the charge and magnetic excitations in both the SC and NSC channels and catalog an assortment of quasiparticle and collective excitations. The present systematic study can guide future RIXS experiments and help to classify compounds as being in the weak- or strong-rung coupling regime, depending on the observed excitations.

Iridates provide another group of spin-$\frac{1}{2}$ ($J_{\rm eff} = \frac{1}{2}$) materials that have been studied with RIXS [46–49]. Moreover, progress was recently made in engineering quasi-1D iridates in heterostructures [50], establishing another platform for examining and controlling the properties of quantum spin ladders. The results presented here can serve as a valuable roadmap in these contexts as well.

Our organization is as follows: Section II introduces the spin ladder model and the relevant scattering cross-sections for RIXS within the Kramers-Heisenberg formalism. Sections III A and III B present results for the RIXS spectra in the NSC and SC channels, respectively. Section III C revisits and discusses the RIXS data reported [5] on the spin-ladder compound $Sr_{14}Cu_{24}O_{41}$ in the context of our results. Section IV summarizes our findings.

II. METHODS

A. Model Hamiltonian

We study the t-J model in a two-leg ladder geometry. The Hamiltonian is

$$\begin{aligned} H = & J_{\rm rung} \sum_i \left(\mathbf{S}_{i,0} \cdot \mathbf{S}_{i,1} - \tfrac{1}{4} n_{i,0} n_{i,1} \right) \\ & + J_{\rm leg} \sum_{i,\tau} \left(\mathbf{S}_{i,\tau} \cdot \mathbf{S}_{i+1,\tau} - \tfrac{1}{4} n_{i,\tau} n_{i+1,\tau} \right) \\ & + t_{\rm rung} \sum_{i,\sigma} \left(c^\dagger_{i,0,\sigma} c_{i,1,\sigma} + \text{h.c.} \right) \\ & + t_{\rm leg} \sum_{i,\tau,\sigma} \left(c^\dagger_{i,\tau,\sigma} c_{i+1,\tau,\sigma} + \text{h.c.} \right). \end{aligned} \tag{1}$$

Here, $\tau = 0,\ 1$ indexes the legs of the ladder while $i = 1, \ldots, L$ indexes the unit cell along each leg; $\mathbf{S}_{i,\tau}$ is a spin operator; $c_{i,\tau,\sigma}$ ($c^\dagger_{i,\tau,\sigma}$) annihilates (creates) a hole with spin σ ($=\uparrow,\downarrow$) at site (i,τ) subject to the constraint of no double occupancy; $J_{\rm leg}$ ($J_{\rm rung}$) and $t_{\rm leg}$ ($t_{\rm rung}$) are the superexchange and hopping integrals along the leg (rung) direction of the ladder, respectively; and $n_{i,\tau} = \sum_\sigma c^\dagger_{i,\tau,\sigma} c_{i,\tau,\sigma}$ is the hole number operator.

Material	$J_{\rm leg}$	$J_{\rm rung}$	$J_{\rm ring}$	Ref.
$Sr_{14}Cu_{24}O_{41}$	130	72		INS [13].
	110	140		RIXS [5].
	110 ± 20	$4J_{\rm leg}/5$		Raman [51].
	145	123		This work.
$La_4Sr_{10}Cu_{24}O_{41}$	186	124	31	INS [23].
$La_6Ca_8Cu_{24}O_{41}$	110	110	16.5	INS [14].
$CaCu_2O_3$	134	11		RIXS [42].

TABLE I. Different values of the exchange parameters (in units of meV) reported in the literature for various spin-$\frac{1}{2}$ ladder systems. Entries where the value of $J_{\rm ring}$ is missing correspond to studies where the ring exchange terms were not included in the analysis.

Note that we neglected the ring-exchange terms in our model for simplicity.

The two-leg spin-ladder model can be used to describe several compounds, and a range of model parameters have been reported, as summarized in Table I. The parameters can be different even for the same compound depending on the nature of the experiment or model used to analyze the data. Due to the variability in the reported couplings, we opted to carry out a systematic study over a range of rung parameters spanning from *weak* to *strong* rung couplings. Unless otherwise stated, we adopt the specific couplings (in units of meV) $J_{\rm leg} = 140$, $J_{\rm rung} = 140r$, $t_{\rm leg} = -300$, and $t_{\rm rung} = -300\sqrt{r}$, where $r = \frac{J_{\rm rung}}{J_{\rm leg}}$ is a parameter used to adjust the ratio of the rung-leg couplings. The choice $t_{\rm rung} = -300\sqrt{r}$ preserves the relationship $J_{\rm rung} \propto \frac{t^2_{\rm rung}}{U}$, assuming a fixed value of U.

B. RIXS Intensity

We evaluated the RIXS response at the Cu L-edge of cuprate materials. In a RIXS experiment, photons with energy $\omega_{\rm in}$ and momentum $\mathbf{k}_{\rm in}$ ($\hbar = 1$) scatter inelastically from a sample, transferring momentum $\mathbf{q} = \mathbf{k}_{\rm out} - \mathbf{k}_{\rm in}$ and energy $\omega = \omega_{\rm out} - \omega_{\rm in}$ to its elementary excitations. The RIXS spectrum is evaluated using the Kramers-Heisenberg formula [52] and is given by

$$\mathcal{I} = \sum_f \left| \frac{\langle f | \mathcal{D}^\dagger_{\mathbf{k}_{\rm out}} | n \rangle \langle n | \mathcal{D}_{\mathbf{k}_{\rm in}} | g \rangle}{E_g + \omega_{\rm in} - E_n + i\Gamma} \right|^2 \delta(E_f - E_g + \omega), \tag{2}$$

where $|g\rangle, |n\rangle$, and $|f\rangle$ are the ground, intermediate, and final states with energies E_g, E_n, and E_f, respectively, and Γ is the core-hole lifetime broadening. The eigenstates are obtained by diagonalizing $H + H_{\rm ch}$, where $H_{\rm ch} = V_c \sum_{i,\tau} n_{i,\tau} n^p_{i,\tau}$ accounts for the interaction between the valence and the core holes in the intermediate state. Here, V_c is the inter-orbital repulsion between the holes in the Cu $2p$ and $3d$ orbitals, $n^p_{i,\tau} =$

$\sum_{m_J} p^\dagger_{i,\tau,m_J} p_{i,\tau,m_J}$, and $p^\dagger_{i,\tau,m_J}$ (p_{i,τ,m_J}) creates (annihilates) a hole in the $m_J = \pm\frac{3}{2}, \pm\frac{1}{2}$ ($m_J = \pm\frac{1}{2}$) states of the $J = \frac{3}{2}$ ($J = \frac{1}{2}$) manifold in the core level of site (i, τ) for L_3 (L_2)-edge. In the two-leg t-J ladder, the dipole operator is given by $\mathcal{D}_{\mathbf{k}} = \sum_{i,\tau,\sigma,m_J} e^{i\mathbf{k}\cdot\mathbf{R}_{i,\tau}} [c_{i,\tau,\sigma} p^\dagger_{i,\tau,m_J} +$ h.c.], where we have neglected the prefactor that depends on the polarization of the photon and the scattering angle. Due to the large spin-orbit coupling in the core $2p$ orbital, both NSC ($\Delta S = 1$) and SC ($\Delta S = 0$) excitations can occur in this edge, [35, 41, 43] and the RIXS spectra has contributions from both of these channels. However, it has been recently shown how the Cu L_3-edge spectra can be resolved into its individual SC and NSC components [41]. For this reason, we will consider these two channels separately in what follows.

The momentum transfer has two components in a two-leg ladder geometry: $\mathbf{q} = (q_x, q_y)$, where $q_x = 2\pi n/La$, with $n \in [0, L)$ but $q_y = 0$ or π/a, only. For our ED calculations, we evaluate Eq. (2) directly, while the details of our DMRG approach are given in Ref. 43.

Throughout this study, we use $V_c = 6.7t$, $\Gamma = |t|$ for all n, and a Lorentzian broadening with $\eta = J_{\rm leg}/6$ for the energy-conserving delta function appearing in Eq. (2), unless stated otherwise. These parameters are typical for Cu L-edge measurements on the cuprates. Most of the spectra were computed using ED on $N = L \times 2 = 10 \times 2$ clusters with periodic boundary conditions, while DMRG was used on $N = L \times 2 = 16 \times 2$ undoped clusters with open boundary conditions. For the doped cases, our ED results are for a filling of $\langle n \rangle = 0.9$ (or 10% doping). Due to the finite size of the lattice, we have discrete peak-like structure in our RIXS plots instead of smooth dispersions, both along momentum and energy axis. Nevertheless, as will become clear in our analysis, the computed RIXS response of small size systems still captures the correct energy scales of the excitations as evident from the comparison with the overlays evaluated from other methods with better momentum resolution.

Finally, the incident photon energy $\omega_{\rm in}$ was tuned to match the maximum of the x-ray absorption spectrum, as discussed in Appendix B.

III. RESULTS AND DISCUSSION

We calculated the RIXS spectra in various rung coupling regimes, ranging from *strong* ($r = \frac{J_{\rm rung}}{J_{\rm leg}} = 4, 2$), to *isotropic* ($r = 1$), to *weak* ($r = 0.5, 0.25, 0.1$). But before examining our results, it is worthwhile to review the various excitations that are expected in a two-leg spin-ladder system.

The magnetic excitations of undoped spin-$\frac{1}{2}$ ladders in the *strong* rung coupling limit are well understood starting from a dimerized rung basis [22, 53]. For $r \to \infty$, the individual rungs of the ladder are decoupled, each forming a spin dimer. For the antiferromagnetic case, the ground state of the L-rung ladder is then a direct product

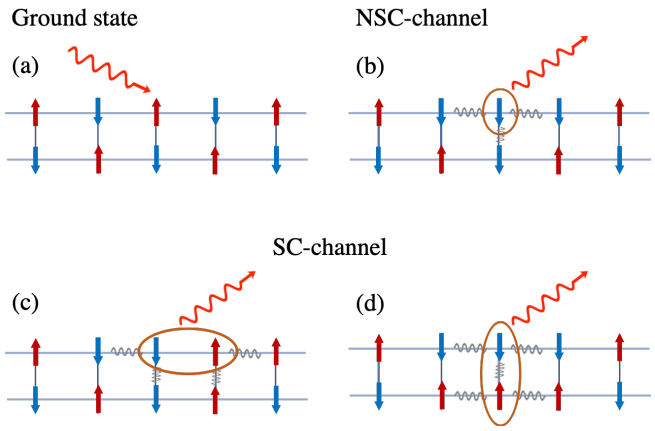

FIG. 1. Schematic diagrams of the elementary magnetic excitations that are possible in spin-ladders. Panel (a) shows the ground state configuration of the spins with antiferromagnetic correlations. Panel (b) shows the single spin-flip excitations that appear in the non-spin-conserving (NSC) channel. Panels (c) and (d) show the double spin-flip processes relevant to the spin-conserving channel (SC). In each panel, the wiggly grey lines indicate "broken" magnetic bonds.

of rung singlets with total spin $S = 0$. The elementary excitations of this state are "triplons" [54–56], where one or more of the rungs are excited into the triplet manifold [57]. For example, the first excited state is L-fold degenerate, where one of the rungs is in a triplet spin configuration, while the higher lying excited states involve integer numbers of rung triplets distributed throughout the system. The degeneracy of the excited states is lifted when $J_{\rm leg} \neq 0$, leading to a dispersive quasiparticle excitation. To order $\mathcal{O}\left(J^2_{\rm leg}/J_{\rm rung}\right)$, the triplon dispersion is [56]

$$\omega_t(q) = J_{\rm rung}\left[1 + \frac{1}{r}\cos(qa) + \frac{3}{4r^2}\right], \tag{3}$$

where a is the lattice constant along the leg direction.

The two-triplon excitation manifold is even richer. Here, the two-triplon excitations appear in three angular momentum channels corresponding to $S = 0, 1, 2$, namely the *singlet*, *triplet* and *quintet* channels, respectively [53, 58, 59]. Previous work [58] showed that a finite value of $J_{\rm leg}$ can lead to two-triplon bound states whose dispersions in the singlet ($S = 0$) and triplet ($S = 1$) channels are to order $\mathcal{O}\left(J^3_{\rm leg}/J^2_{\rm rung}\right)$ given by [53]

$$\omega^S_{2t}(q) = J_{\rm rung}\Big[2 - \tfrac{3}{2r} + \tfrac{19}{16r^2} - \tfrac{9}{32r^3} - \left(\tfrac{1}{2r} - \tfrac{1}{8r^2} + \tfrac{51}{128r^3}\right) \times \cos(qa) - \left(\tfrac{5}{16r^2} + \tfrac{21}{32r^3}\right)\cos(2qa) - \tfrac{37}{128r^3}\cos(3qa)\Big], \tag{4}$$

and

$$\omega_{2t}^{T}(q) = J_{\rm rung}\Big[2 - \tfrac{3}{2r} + \tfrac{11}{8r^2} + \tfrac{17}{16r^3} - \big(\tfrac{1}{r} + \tfrac{1}{4r^2} - \tfrac{9}{16r^3}\big) \times \cos(qa) - \big(\tfrac{1}{2r^2} + \tfrac{1}{2r^3}\big)\cos(2qa) - \tfrac{5}{16r^3}\cos(3qa)\Big], \quad (5)$$

respectively.

The two-triplon excitations in the *triplet* channel were analyzed in a recent INS study [23], reporting a dispersive excitation along the $\mathbf{q} = (q_x, 0)$ direction in the Brillouin zone, in very good agreement with the *lower boundary* line of the two-triplon continuum. It was also argued that the four-spin ring-exchange term frustrates the formation of a $S = 1$ bound state below the continuum. In this effort, we neglect the four-spin cyclic exchange, thus we find that our data overlays well with the dispersion of the bound $S = 1$ two-triplon state. Our results are also consistent with the available RIXS experimental data [5]. We know of no experimental study probing two-triplon excitations in the *singlet* and *quintet* channels; however, our results below show that the RIXS SC channel can access the two-triplon bound state in the *singlet* channel.

In the *weak* rung coupling limit for undoped two-leg spin-$\frac{1}{2}$ ladders, the system can be viewed as a set of weakly coupled Heisenberg chains. In this regime, the excitation spectrum is understood in terms of a confined spinon continuum with a finite spin gap [60]. Intuitively, the excitations of a Heisenberg chain are spin-$\frac{1}{2}$ spinons, which always appear in pairs and are basically free to move along a single chain. When the two chains are coupled antiferromagnetically, however, the spinons within a single chain feel an effective confining potential [2]. This potential is created by the region of ferromagnetically coupled spins that forms on the rungs between the two spinons as they separate.

When $r \ll 1$, the two-leg ladder problem can be mapped onto one of weakly interacting *singlet* and *triplet* Majorana fermions with effective masses $m_s = 3m$ and $m_t = m$, respectively, where $m \approx 0.41 J_{\rm rung}$ [61]. The excitation spectrum, as encoded in the dynamical spin structure factor $S(q, \omega)$ [11], is characterized by combination of sharp modes and a broader continuum arising from several multi-particle Majorana excitations. The lower boundaries of these excitations are defined by

$$\omega_l(q) \approx \sqrt{m_{\rm thres}^2 + v^2(q_x - q_x^{\rm min})}, \quad (6)$$

where $v = \frac{\pi J_{\rm leg}}{2}$ is the spin velocity of the chain and $m_{\rm thres}$ and $\mathbf{q}^{\rm min}$ depend on the particles involved in the excitation. A summary of the relevant values can be found in Table I of Ref. 11, which we have reproduced in Table II for convenience. From this table, one can see that a Majorana triplet (1T) excitation appears near $\mathbf{q}^{\rm min} = (\pi/a, \pi/a)$ and $m_{\rm thres} = m$, while the excitations near $\mathbf{q}^{\rm min} = (\pi/a, 0)$ correspond to a three-particle bound state consisting of two Majorana triplets and a Majorana singlet (2T + 1S) with a threshold set by $m_{\rm thres} = 5m$. While the mapping to the Majorana fermion picture holds for $r \ll 1$, recent DMRG results for $S(q, \omega)$ [11] have shown that this picture provides a qualitative description of the excitation spectrum for a wide range of $r < 1$. These same calculations also showed that the spectral weight of the multi-particle continuum increases as $r \to 0$ until the entire excitation spectrum converges to the expected two-spinon continuum of the antiferromagnetic Heisenberg chain with lower and upper boundaries given by $\omega_s^l(q) = \frac{\pi}{2} J\,|\sin(qa)|$ and $\omega_s^u(q) = \pi J\,|\sin(qa/2)|$, respectively.

Excitation	$\mathbf{q}^{\rm min}$	m_{thres}
1T	$(\pi/a, \pi/a)$	$1m$
2T	$(0, 0)$	$2m$
3T	$(\pi/a, \pi/a)$	$3m$
1T + 1S	$(0, \pi/a)$	$4m$
2T + 1S	$(\pi/a, 0)$	$5m$

TABLE II. The momentum $\mathbf{q}^{\rm min}$ and m_{thres} values that define the lower boundaries of the single- and multiparticle excitations that occur in the Majorana fermion description of the spin-$\frac{1}{2}$ ladders. Reproduced from Ref. 11.

Understanding the behavior of a small number of holes doped into an antiferromagnetic background is one of the central problems in the quest to comprehend unconventional superconductivity. In this context less is known about the excitations in doped spin-ladders as compared to the undoped case, where the former are usually studied using numerical methods [22, 62–66]. A single hole doped into a two-leg ladder introduces a spin $\frac{1}{2}$ and charge $+e$ to the system. DMRG results [63] indicate that in the strong-rung coupling limit, the doped hole behaves as a quasiparticle, where the spin and charge remain tightly bound within a typical distance of about one lattice constant. In the isotropic limit, the quasiparticle develops more internal structure with a length scale of $\sim 3a$. In the decoupled case ($J_{\rm rung} = 0$), the doped hole fractionalizes completely into a spinon and holon [36, 67].

In the analysis below, we explore the RIXS spectra in both the NSC and SC channels and identify the relevant elementary excitations in these spectra.

A. Results for the non-spin-conserving channel

We begin our study with the NSC or "spin-flip" channel, which typically dominates the Cu L-edge RIXS spectra in cuprates [41, 68]. The NSC channel produces local single spin-flips due to a large spin-orbit coupling in the $2p$ core level, as shown in Fig 1(b). The elementary excitations generated in this scattering channel correspond to magnetic excitations with $\Delta S = 1$ relative to the ground state. In terms of the spectra, the NSC channel is comparable to the spin-flip channel of INS, and hence RIXS spectra at the Cu L-edge of cuprates compare well with

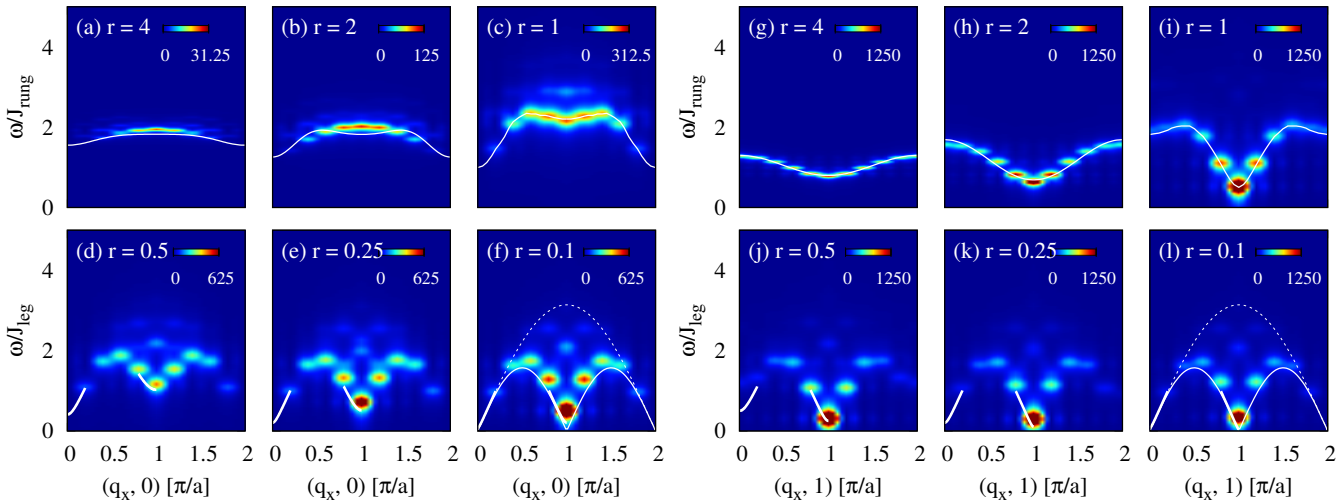

FIG. 2. The RIXS spectra in the non-spin-conserving channel for a half-filled t-J ladder, using ED and a 2×10 cluster. $I^{\Delta S=1}(q_x, 0, \omega)$ and $I^{\Delta S=1}(q_x, \pi/a, \omega)$ are shown in panels (a)-(f) and (g)-(l), respectively. Panels (a)-(c) and (g)-(i) have overlays of the dispersion relationships for the bound *triplet* two-triplon [Eq. (5)] and the one-triplon excitations [Eq. (3)], respectively, calculated using perturbation theory. Panels (c) and (i) have overlays (solid white) of the dispersion relationships for the same excitations extracted from Ref. 55, which were evaluated using a continuous unitary transformation (CUT) method. The thin dotted and solid white lines in panels (f) and (l) plot the upper and lower boundaries of the two spinon continuum expected for completely decoupled chains. The thick white lines in panels (d)-(f) and (j)-(l) plot the lower boundaries of the multiparticle continua near their respective minima. Note that the y-axis of the top and botton rows are scaled with respect to $J_{\rm rung}$ and $J_{\rm leg}$, respectively.

$S(\mathbf{q}, \omega)$ (see Appendix A) [37, 68].

1. *Undoped t-J ladders*

The RIXS spectra in the NSC channel for undoped ladders are plotted in Fig. 2. Panels (a)-(f) and (g)-(l) show results for momentum transfers $\mathbf{q} = (q_x, 0)$ and $\mathbf{q} = (q_x, \pi/a)$, respectively. Several excitations are identified.

In the limit of strong rung coupling, the spectra along the $\mathbf{q} = (q_x, 0)$ direction [Figs. 2(a) and 2(b)] exhibit a dispersive quasiparticle-like excitation. To determine its nature, we overlayed the dispersion $\omega_{2t}^T(q)$ given by Eq. (5). We find that the observed excitation closely follows the dispersion relationship for $r = 4$ but for $r = 2$ there are some deviations, most notably at the zone boundary. (The disagreement becomes even more apparent for $r = 1$, as discussed below.) The agreement between the dispersion of the excitations and $\omega_{2t}^T(q)$, and the fact that we are in the NSC channel, allows us to conclude that these excitations are the two-triplon bound state in the *triplet* channel. Similarily, the $\mathbf{q} = (q_x, \pi/a)$ excitation in the strong-rung coupling case [Figs. 2(g) and 2(h)] corresponds to a single triplon excitation. To confirm this, we overlayed the dispersion $\omega_t(q)$ given by Eq. (3), showing it captures well the observed excitations for $r \geq 2$.

As discussed in the previous section, in the weak-rung coupling limit we expect the legs of the ladders to behave as weakly coupled antiferromagnetic chains. Indeed, along both the $(q_x, 0)$ [Figs. 2(d)-(f)] and $(q_x, \pi/a)$ [Figs. 2(j)-(l)] directions, the spectra can be described using the picture of confined spinons with a continuum of excitations appearing above a sharper dispersing mode. The lower boundaries of the continua near their respective minima are overlaid as thick white lines. According to Table II, we assign the excitations near $\mathbf{q}^{\rm min} = (0, 0)$ to 2T excitations with $m_{\rm thres} = 2m$, while the excitations near $\mathbf{q}^{\rm min} = (\pi/a, 0)$ correspond the 2T + 1S excitations with $m_{\rm thres} = 5m$. Similarily, the excitations near $\mathbf{q}^{\rm min} = (\pi/a, \pi/a)$ are 1T excitations with $m_{\rm thres} = m$ and the excitations near $\mathbf{q}^{\rm min} = (0, \pi/a)$ correspond to 1T + 1S excitations with $m_{\rm thres} \approx 4m$.

The *isotropic* coupling case behaves qualitatively like the strong-rung coupling cases, but the calculated spectra deviate significantly from the dispersion predicted by perturbation theory [Eq. (5)]. Nevertheless, we are still able to assign the intense dispersing features to the $S = 1$ two-triplon bound state and the one-triplon excitations, as in the strong-rung coupling limit. In Fig. 2(c) and Fig. 2(i) we have overlayed the dispersions for the bound *triplet* two-triplon and one-triplon excitations, respectively, this time extracted from Fig. 4 of Ref. 55. In this case, the dispersions were computed using a continuous unitary transformation (CUT) method, and agree well with our evaluated spectra. In Fig. 2(c) we also observe additional spectral weight at higher energies, which corresponds to the two-triplon continuum. Our results in this regime should be of considerable interest for future RIXS experiments on cuprates spin-$\frac{1}{2}$ ladder materials, as most of

the estimated values of the $J_{\rm rung}/J_{\rm leg}$ ratios fall in this intermediate category.

2. Doped t-J ladders

The excitations of doped ladder compounds are relevant to explain pressure-induced superconductivity. Moreover, while low-energy spin-fluctuations are widely considered pivotal for superconductivity, the relationship between the doping evolution of charge and high-energy spin excitations and the superconducting mechanism has recently become the subject of considerable debate, especially in 2D cuprates. Our results for the RIXS spectra of the doped spin-ladder in the NSC-channel are in Fig. 3. As in the undoped case, panels (a)-(f) and (g)-(l) show spectra along the $(q_x, 0)$ and $(q_x, \pi/a)$ directions, respectively.

For strong-rung couplings [Figs. 3(a) and 3(b)], the spectra along the $\mathbf{q} = (q_x, 0)$ directions have two distinct sets of excitations. The first corresponds to the same *triplet* two-triplon excitations identified in the undoped case, as confirmed by overlaying the dispersion given by Eq. (5) as solid white lines. The second is the Bloch quasiparticle excitation formed from the tightly bound spin and charge of the doped hole [63]. Its dispersion is well described by $\omega(k) = 2\tilde{t}[1 - \cos(ka)]$ (the dashed line overlay), where $\tilde{t} = t_{\rm rung}/2$ is the effective hopping of a quasiparticle in the bonding band [62]. The fact that the spectra exhibits gapless charge and gapped spin (C1S0) excitations is consistent with the system's classification as a Luther-Emery liquid [62, 69]. The spectra along the $\mathbf{q} = (q_x, \pi/a)$ direction, shown in Figs. 3(g) and 3(h), have only a single set of excitations, whose dispersions agree well with the one-triplon excitation Eq. (3), which is again overlaided as a solid white line.

Results for the weak-rung coupling regime along the $\mathbf{q} = (q_x, 0)$ and $(q_x, \pi/a)$ directions are shown in Figs. 3(d)-(f) and Figs. 3(j)-(l), respectively. We find that the spectra soften as compared to undoped spin ladders. Moreover, the spin gap no longer appears to scale with $J_{\rm rung}$ but instead appears to vanish at $(\pi/a, 0)$ for all $r < 1$ while persisting at $\mathbf{q} = (\pi/a, \pi/a)$.

In the *isotropic* case at $\mathbf{q} = (0, \pi/a)$, shown in Fig. 3(c), the brightest dispersing peak does not have the same downturn in the two-triplon dispersion that was observed in the undoped case. Instead, there is an increased weight appearing in at higher energy losses, corresponding to the two-triplon continuum. In contrast, the excitations at $\mathbf{q} = (\pi/a, \pi/a)$, shown in Fig. 3(i), have the ubiquitous incommensurate peaks that are also commonly observed in doped ladders and 2D cuprates [66, 70–72]. It is interesting to contrast the results for the doped two-leg spin ladder found above with available results in the doped 2D cuprates at the Cu L-edge. In 2D cuprates, a weakly dispersive high-energy paramagnon band along the $\mathbf{q} = (q_x, 0)$ line was reported to be persistent upon hole doping [26–29, 37]. This type of excitation compares relatively well with our results in the two-leg ladder case in Fig. 3(c) for the isotropic case.

B. Results for the spin-conserving channel

We now analyze the RIXS spectra in the SC channel, both for the undoped and doped cases. As shown pictorially in Figs. 1(c) and 1(d), the magnetic excitations that are accessible in this channel occur via double spin-flip processes, which correspond to $\Delta S = 0$ excitations in the antiferromagnetic ladders. For the undoped cuprates measured at the Cu L-edge, the SC channel probes excitations encoded in the dynamical exchange structure factor $S^{\rm exch}(\mathbf{q}, \omega)$ (see Appendix A), which is a second order term in the ultrashort core-hole lifetime (UCL) expansion [34, 68]. The fact that $S^{\rm exch}(\mathbf{q}, \omega)$ captures most of the RIXS intensity indicates that magnetic excitations in this channel are dominated by double spin-flip processes. Because these are higher order processes, this channel is expected to be weaker as compared to the NSC channel, [41, 68] and our results are consistent with this expectation. In the doped case, magnetic and charge excitations coexist in the RIXS spectra and the SC channel also has a significant contribution at second order given by a modified charge structure factor $\tilde{N}(\mathbf{q}, \omega)$ [see Eq. (9) of Ref. 68 and Appendix A]. The SC channel is also particularly relevant at the O and Cu K-edges, where direct spin-flip excitations are often forbidden [4, 25, 36]. Our numerical study motivates RIXS experiments that could be able to disentangle SC and NSC components of the spectra by the use of photon polarization, which has been successfully demonstrated in Ref. 41 for the weakly coupled ladder cuprate $CaCu_2O_3$.

1. Undoped t-J ladders

The RIXS spectra in the SC channel for the undoped ladders are shown in Fig. 4. Panels (a)-(f) and (g)-(l) show the RIXS spectra for momentum transfers along the $\mathbf{q} = (q_x, 0)$ and $(q_x, \pi/a)$ directions, respectively. As expected, the intensity of the excitations in this channel is weaker as compared to the NSC channel by approximately one order of magnitude.

As with the previous sections, we first consider the strong-rung coupling limit. Along the $(q_x, 0)$ direction [Figs. 4(a) and 4(b)], we observe a weakly dispersing feature that agrees well with the two-triplon bound state in the *singlet* channel given by Eq. (4). This is one of the important results of our current investigation: because the SC channel probes $\Delta S = 0$ excitations, we are able to clearly identify and distinguish the two-triplon bound states in both the singlet and triplet channels. We also see additional spectral weight at higher binding energies near $(\pi/a, 0)$, which contrasts qualitatively with the results in the weak-rung coupling limit. This weight falls

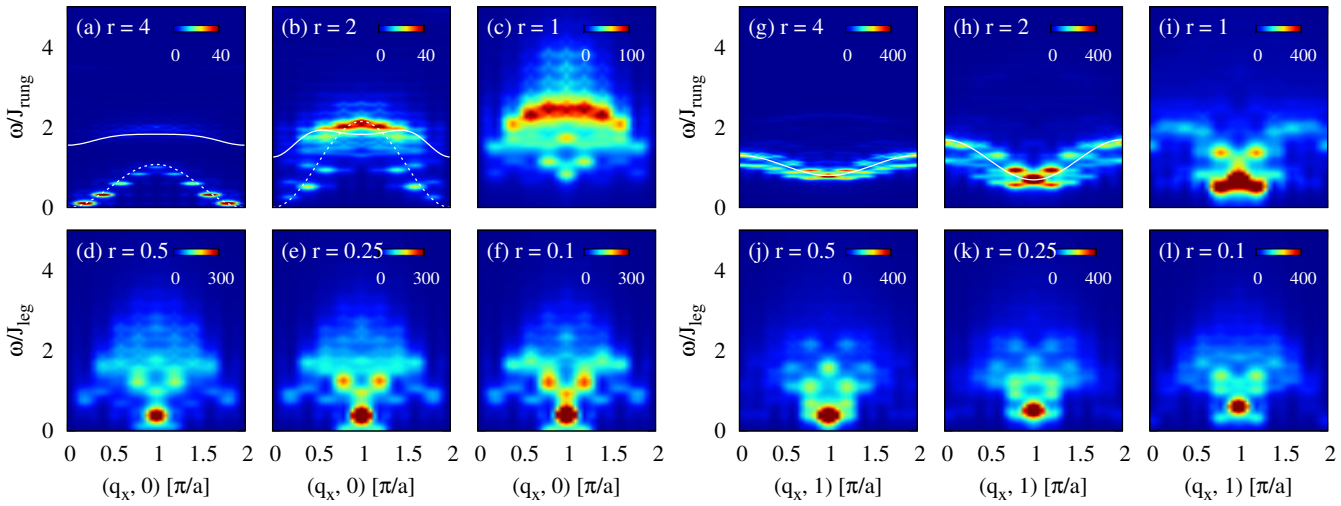

FIG. 3. RIXS spectra in the non-spin-conserving channel for a doped t-J ladder, using ED on a 2×10 cluster and a filling of $\langle n \rangle = 0.9$. $I^{\Delta S=1}(q_x, 0, \omega)$ and $I^{\Delta S=1}(q_x, \pi/a, \omega)$ are in panels (a)-(f) and (g)-(l), respectively. Panels (a), (b) and (g), (h) have overlays (solid white) of the dispersion relationships for the bound *triplet* two-triplon [Eq. (5)] and one-triplon excitations [Eq. (3)], respectively, derived using perturbation theory. Panels (a) and (b) have an additional overly (dashed white) of the dispersion for a quasiparticle $\omega(k) = 2\tilde{t}[1 - \cos(ka)]$. The y-axis of the top and botton rows are scaled with respect to $J_{\rm rung}$ and $J_{\rm leg}$, respectively.

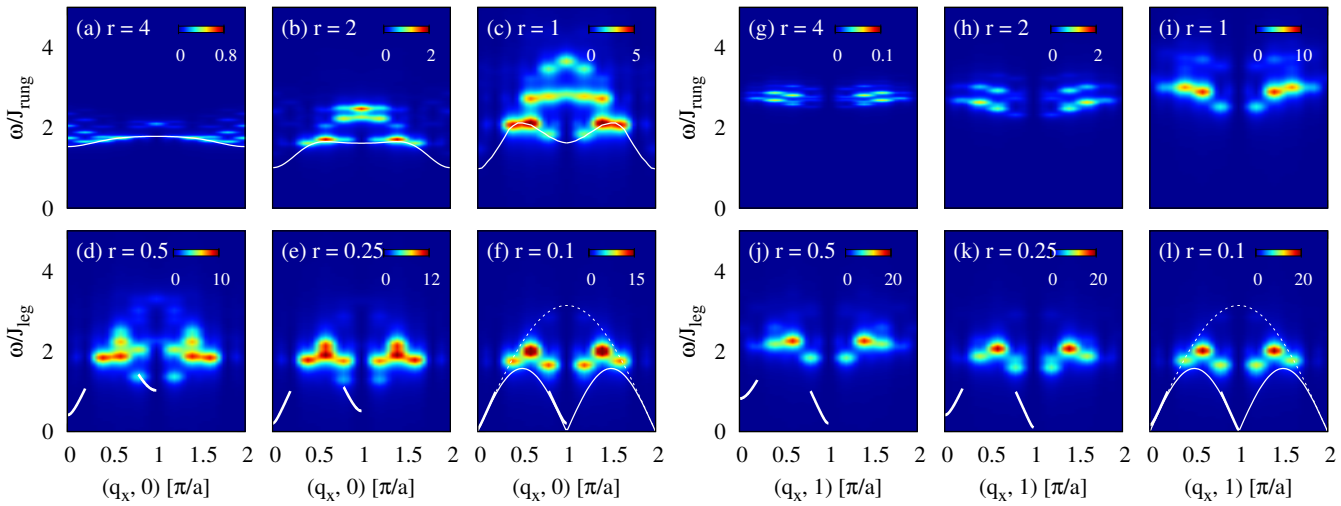

FIG. 4. RIXS spectra in the spin-conserving channel for the half-filled t-J ladder, using ED and a 2×10 cluster. $I^{\Delta S=0}(q_x, 0, \omega)$ and $I^{\Delta S=0}(q_x, \pi/a, \omega)$ are in panels (a)-(f) and (g)-(l), respectively. Panels (a) and (b) have overlays (solid white) of the dispersion relations of the *singlet* bound two-triplon excitations [Eq. (4)] derived using perturbation theory, while panel (c) has an overlay of the dispersion relation for the same excitation from Ref. 55, using the CUT method. The thin dotted and solid white lines in panels (f) and (l) plot the upper and lower boundaries of the two spinon continuum expected for completely decoupled chains. The thick white lines in panels (d)-(f) and (j)-(l) plot the lower boundaries of the multiparticle continua near their respective minima. The y-axis of the top and botton rows are plotted in units of $J_{\rm rung}$ and $J_{\rm leg}$, respectively.

within the two-triplon continuum and likely corresponds to two-triplon continuum in the singlet channel.

Along the $\mathbf{q} = (q_x, \pi/a)$ direction in the strong-rung coupling regime shown in panels (g) and (h), the spectra can again be understood as multiparticle excitations in the *singlet* channel, which we observe at energy losses around $3J_{\rm rung}$. Further analysis of these excitations using strong-coupling series expansion methods are desirable [53]. We observe zero spectral weight at $(\pi/a, \pi/a)$ for all the rung couplings we investigated, in contrast to the weak spectral weight observed at $(\pi/a, 0)$. The nature of these excitations can be qualitatively captured using the dynamical exchange structure factor $S^{\rm exch}(\mathbf{q}, \omega)$, which has been computed and shown in Fig. 9 of Appendix A. Indeed, $S^{\rm exch}(\mathbf{q}, \omega)$ shows the spectral weight cancellation at $(\pi/a, \pi/a)$ for all the rung couplings in-

vestigated.

In the weak rung regime ($r < 1$), the spectra along $\mathbf{q} = (q_x, 0)$ and $(q_x, \pi/a)$, shown in Figs. 4(d)-(f) and 4(j)-(l), respectively, resemble the continuum expected for confined spinons also observed in the NSC channel. To highlight this, we overlaid the boundaries of the two-spinon continuum as well as the lower boundaries of the multi-particle continua that were introduced when describing the NSC channel. In this case, all of the excitations appear above the lower boundary lines, indicating that these excitations are multiparticle in nature. We also note that spectra along both momentum directions have a suppressed intensity at $q_x = \pi/a$, which is similar to what occurs in one-dimensional antiferromagnetic chains when probed in the SC channel [35, 73, 74].

The spectra along both momentum directions for the isotropic case ($r = 1$) behaves qualitatively similar to the strong-rung coupling case, where we observe a continuum of excitations. In Fig. 4c, we plot an overlay extracted from Fig. 4(b) of Ref. 55 for bound two-triplon excitation in the *singlet* channel, again evaluated using the CUT method. This dispersion agrees well with the lower boundary of the evaluated spectra suggesting that the continuum of excitations is related to *singlet* two-triplon excitations and that the bound singlet state is not far removed from the continuum.

2. Doped t-J ladders

Finally, we examine the RIXS spectra of the doped ladders in the SC channel. As before, Figs. 5(a)-(f) and 5(g)-(l) show results for momentum transfers $\mathbf{q} = (q_x, 0)$ and $(q_x, \pi/a)$, respectively. The spectra are quite rich and we observe several new excitations that were not present in the undoped ladders. Indeed, we expect that magnetic and charge excitations coexist in the SC channel response and that most of the spectral features observed in the full RIXS response can be described using the modified dynamical charge correlation function $\tilde{N}(\mathbf{q}, \omega)$ (see Fig. 10 in Appendix A and Ref. 68).

As before, we begin our discussion from the strong-rung coupling limit. In this case, the ladder can be considered as composed of weakly decoupled dimers where the orbitals on each leg form bonding and antibonding states. If $t_{\rm leg}$ is finite, these bonding (-) and antibonding (+) states form the basis for Bloch states with dispersion relations given by $\omega(q) = \mp t_{\rm rung} + 2\tilde{t}[1 - \cos(qa)]$ [62], where $\tilde{t}$ is the effective hopping parameter obtained from the change of basis to the bonding and antibonding states. When a small number of holes are doped into the system, they first occupy the bonding band as quasiparticles, as shown in Fig. 6. The charge excitations observed in this channel can then be understood by invoking quasiparticle scattering within and between the bonding and antibonding bands, respectively.

Along the $(q_x, 0)$ direction in the strong-rung coupling regime, Figs. 5(a) and 5(b), we observe dispersive charge excitations consistent with particle-hole scattering within the bonding band, as shown in Fig. 6. To confirm this, we overlaid the dispersion $\omega(q) = 2\tilde{t}[1 - \cos(qa)]$, where $\tilde{t} \approx t_{\rm leg}/2$, which agrees with the numerical data [62]. Along the $(q_x, \pi/a)$ direction [Figs. 5(g) and 5(h)] we find the corresponding particle-hole excitation where scattering occurs into the antibonding band. In this case, we overlaid the dispersion $\omega(q) = 2t_{\rm rung} + 2\tilde{t}[1 - \cos(qa)]$ (white dashed line). We also notice that the bonding and anti-bonding band are separated by $2t_{\rm rung}$, which accounts for the shift in cosine-like dispersion observed when $q_y = \pi/a$.

It is important to note that, even in this case, these charge excitations are weaker in intensity when compared to the magnetic excitations in NSC channel by approximately one order of magnitude, but stronger than the SC channel of the undoped case. Our results show that RIXS can explicitly probe charge excitations at low energies as suggested in the literature for the Cu L_3-edge [75, 76].

In addition to the charge excitations, we also observe a continuum of magnetic excitations for momentum transfers along $(q_x, \pi/a)$. The lower boundary of this continuum is defined by the one triplon dispersion given by Eq. (3), which has been overlaid as a dotted white line.

In the weak-rung coupling regime, shown in Figs. 6(d)-(f) and 6(j)-(l), the quasiparticle excitations display a bandwidth $4t_{\rm leg}$ with dispersion $\omega(q) = 2t_{\rm leg}[1 - \cos(qa)]$ along both the $(q_x, 0)$ and $(q_x, \pi/a)$ directions. This is similar to the results for the 1D AFM chain reported in Ref. 36 where the excitations are holons, and consistent with the notion that the individual legs of the ladder are weakly coupled. The fact that these observed excitations are completely governed by $t_{\rm leg}$ indicates that the holes occupy the chains of the ladder rather than the bonding and antibonding orbitals on each rung.

Finally, we consider the isotropic rung-coupling limit, which is of much interest for future RIXS experiments and future theoretical investigations. In this case, our spectra show a gapless and a gapped continuum along the $(q_x, 0)$ and $(q_x, \pi/a)$ directions, respectively. These results hence resemble qualitatively the spectral features also observed in the strong-rung coupling limit. It is interesting to compare our full RIXS spectra with the dynamical charge structure factor results reported in Fig. 7 of Ref. 20: our results compare well with the lower Hubbard band excitation observed in which $N(q_x, \pi/a, \omega)$ is gapped, in contrast to the gapless $N(q_x, 0, \omega)$.

C. Revisiting $Sr_{14}Cu_{24}O_{41}$ RIXS data

Cu L_3-edge RIXS data has been reported [5] for the prototypical spin-ladder $Sr_{14}Cu_{24}O_{41}$. At that time, the observed spectra were interpreted in terms of two-triplon $\Delta S = 0$ excitations in the strong rung coupling regime ($r \approx 1.37$) as it was believed that $\Delta S = 1$ excitations were forbidden at the Cu L_3-edge. It was later shown that not only is this channel allowed but that

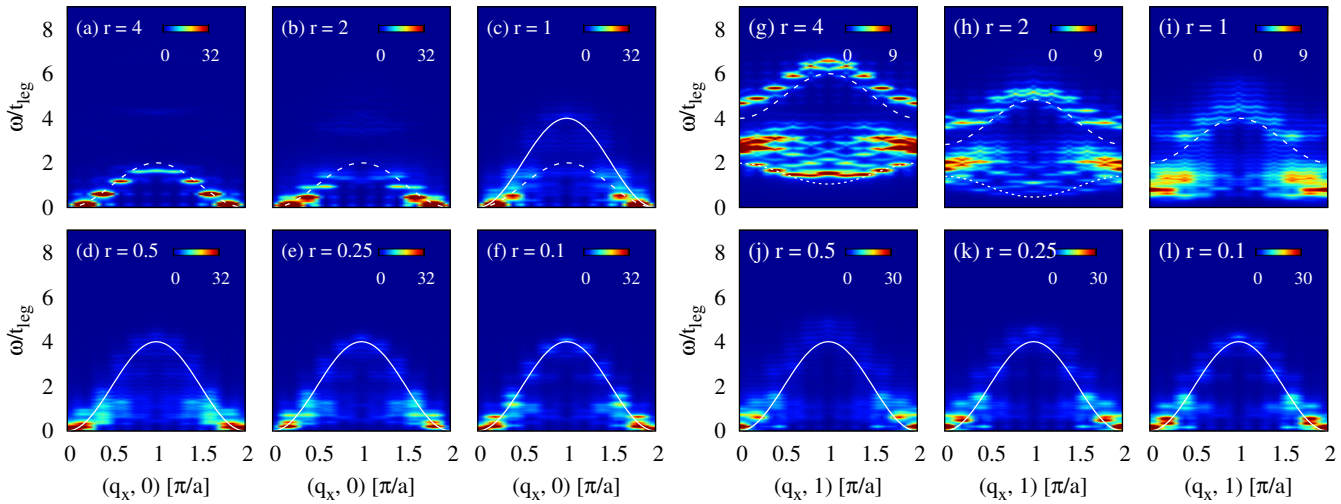

FIG. 5. RIXS spectra in the spin-conserving channel for the doped t-J ladder, using ED, a 2×10 cluster, and $n = 0.9$. $I^{\Delta S=0}(q_x, 0, \omega)$ and $I^{\Delta S=0}(q_x, \pi/a, \omega)$ are in panels (a)-(f) and (g)-(l), respectively. In panels (a)-(c) the dispersions of the quasiparticle state with a bandwidth $W = 2t_{\rm rung}$ are shown (white dashed). In panels (d)-(f) and (j)-(l) the holon dispersion with a bandwidth $W = 4t_{\rm leg}$ is also shown (solid white). The white dashed overlay in panels (g)-(i) plot the boundary of the spinon-holon continuum gapped by $2t_{\rm rung}$, while the dotted overlay in panels (g) and (h) corresponds to the dispersion relation of the one-triplon excitations. The y-axis of the top row and botton rows are plotted in units of $t_{\rm leg}$.

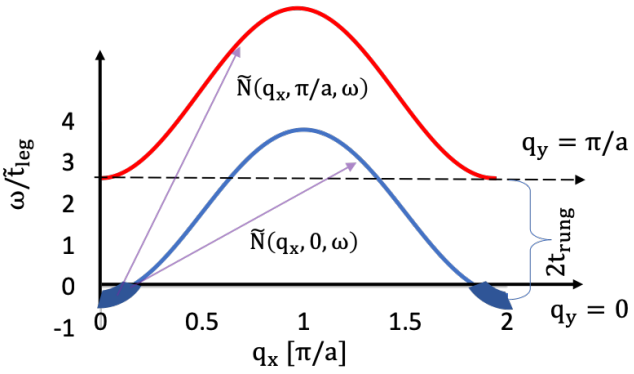

FIG. 6. A schematic diagram of the particle-hole excitations possible in the doped t-J ladder in the weak-rung coupling regime. In this limit, the orbitals along the legs form bonding $\frac{1}{\sqrt{2}}(c^\dagger_{i,\sigma,1} - c^\dagger_{i,\sigma,2})|0\rangle$ and anti-bonding $\frac{1}{\sqrt{2}}(c^\dagger_{i,\sigma,1} + c^\dagger_{i,\sigma,2})|0\rangle$ states, which form the basis for the Bloch states propagating along the leg direction. In this case, the dispersions of the two Bloch states are split by an amount proportional to the rung hopping $\pm t_{\rm rung}$. The doped holes form quasiparticles carrying both spin-$\frac{1}{2}$ and charge e, and the broad blue colour highlights the filled states in the ground state. RIXS probes scattering within the bonding and to the antibonding band, as shown by the arrows.

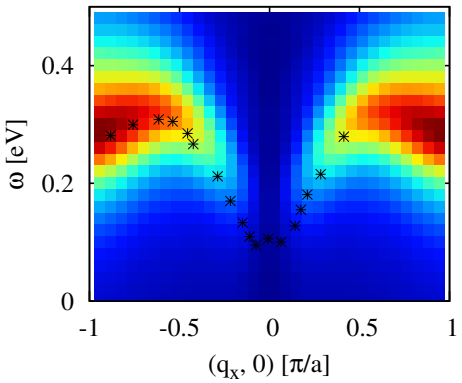

FIG. 7. Calculated RIXS spectra of an undoped t-J ladder in the non-spin-conserving channel $I^{\Delta S=1}(q_x, 0, \omega)$ evaluated using DMRG on an $N = 16 \times 2$ lattice. The black squares overlay the peak positions of the spectra extracted from the experimental Cu L_3-edge data for $Sr_{14}Cu_{24}O_{41}$, reproduced from Ref. 5.

it dominates the magnetic RIXS response in the undoped cuprates [31]. The RIXS spectra were later theoretically evaluated [8] employing a projection method for the two-leg ladder using the parameter set derived from $La_4Sr_{10}Cu_{24}O_{41}$ in Ref. 23 (the model involved additional ring spin-exchange term as compared to our model). These calculations showed that the RIXS spectra was associated with the two-triplon excitations with $\Delta S = 1$ when momentum transfers of $q_y = 0$ were used, as shown in Fig. 6 of Ref. 8. But there was also a significant difference in the dispersion of the experimental and theoretical data. Armed now with these theoretical insights and our new model calculations, we revisit the existing $Sr_{14}Cu_{24}O_{41}$ data.

To access large system sizes with improved momentum resolution, we computed the RIXS spectra in the $\Delta S = 1$ channel for an undoped spin-ladder using our recently formulated DMRG approach [43]. To obtain a

unified description of RIXS and INS experiments, we first adopted a model given by Eq. (1) without ring exchange terms, however, we found that this model gave poor agreement with the experimentally observed RIXS spectra. Instead, we are able to find good agreement when we set $J_{\rm leg} = 145$ meV and $J_{\rm rung} = 0.85 J_{\rm leg}$. This result places $Sr_{14}Cu_{24}O_{41}$ in the weak rung-coupling regime but close to the isotropic limit. The resulting RIXS spectra shown in Fig. 7 agree well with the experimental data, but the theoretical model predicts a vanishing spectral weight at $q_x = 0$. This observation is consistent with the model of Ref. 8 but inconsistent with the finite intensity observed in the experiment. At this time, the source of this discrepancy is unclear.

Because r is close to the isotropic case, the data can be qualitatively understood using either the dimer excitation picture or the confined spinon picture. In the former case, the excitations are understood as bound $S = 1$ two-triplet excitations. In the latter case, they are viewed as a three particle bound state composed of Majorana fermions near the zone boundary. However, a quantitative description of the data can only be achieved with nonperturbative numerical methods. In this sense, our results place $Sr_{14}Cu_{24}O_{41}$ in a regime similar to the organometallic compound $(C_7H_{10}N)_2CuBr_4$ [11], but with larger exchange couplings.

IV. CONCLUSIONS

We have systematically studied the RIXS spectra of both undoped and doped spin-$\frac{1}{2}$ ladders, covering the weak- to strong-rung coupling regimes. Our study shows that RIXS experiments performed on these compounds can access a wealth of magnetic and charge excitations. This study was motivated by RIXS experiments at the Cu L-edge in low-dimensional cuprates, where the RIXS data can be decomposed into the non-spin-conserving (NSC) and spin conserving (SC) channels [25, 35, 41, 68]. Therefore, we evaluated the RIXS spectra in both of these channels and provided an energy-momentum resolved roadmap that can guide future RIXS experiments on spin-ladder compounds.

In the first part of our effort, we reported the RIXS excitations in the NSC or "spin-flip" channel, which typically dominates the Cu L-edge RIXS spectra in the cuprates [41, 68]. In the undoped two-leg ladder, we have shown that RIXS can access dispersive one triplon excitations and a two-triplon bound state in the *triplet* ($S = 1$) channel in the intermediate to strong rung coupling regime. In the weak-rung coupling regime, the NSC channel probes single- and multiparticle excitations consistent with the Majorana fermion description of confined spinons.

The study of the RIXS spectra for doped spin-$\frac{1}{2}$ ladder compounds is of much importance in the context of pressure-induced superconductivity in low-dimensional high-T_c cuprates. In the doped ladder, we accessed one- and (triplet) two-triplon excitations in the strong-rung coupling limit and softened confined spinons in the weak-rung coupling limit. We also identified signatures of a bound spin-charge quasiparticle excitation in the strong-rung coupling limit.

In the second part of our work, we studied the RIXS spectra of the spin-ladder in the SC channel, which probes $\Delta S = 0$ excitations of the system [41, 68]. This component of the RIXS spectra has received less attention in the literature, and our work provides a starting point for future theoretical and experimental investigations of this channel on spin-ladders. In the undoped ladders, magnetic excitations are created in this channel via double spin-flip processes. Because these are higher order processes, their contribution to the RIXS spectra is expected to be weaker compared to the NSC channel [41, 68]. Our results are consistent with this expectation, and we found that the spectral intensity is at least one order of magnitude smaller than the corresponding spectra in the SC channel. Nevertheless, in the intermediate to strong rung coupling regime, we are able to identify bound two-triplon excitations in the singlet ($S = 0$) channel.

In the SC RIXS channel for doped spin-ladders, we identified a set of dispersive low-energy charge excitations that were interpreted by invoking quasiparticle scattering within and between the bonding and antibonding bands, respectively, in the strong rung coupling case. Conversely, the spectra are dominated by holon excitations in the weak-rung coupling limit. The direct access to charge excitations offered by this channel provides a new opportunity to study superconductivity in cuprate ladders, where the role of spin and charge excitations is still debated. We believe our numerical study motivates new RIXS experiments on spin-ladders such as $Sr_{14}Cu_{24}O_{41}$ allowing disentanglement of data into the NSC and SC channels, due to the richness predicted in the RIXS spectra.

Finally, we revisited the available RIXS data for $Sr_{14}Cu_{24}O_{41}$and found that it was best described using a model in the weak rung coupling regime with $r = 0.85$. This result is in contrast to the previous analysis [5] that placed it in the strong rung coupling regime but in qualitative agreement with the INS data [13]. .

ACKNOWLEDGMENTS

We thank T. Schmitt and J. Schlappa for useful discussions. A. N. and E. D. are supported by the U.S. Department of Energy, Office of Science, Basic Energy Sciences, Materials Sciences and Engineering Division. S. J. is supported by the National Science Foundation under Grant No. DMR-1842056. This work used computational resources supported by the University of Tennessee and Oak Ridge National Laboratory Joint Institute for Computational Sciences.

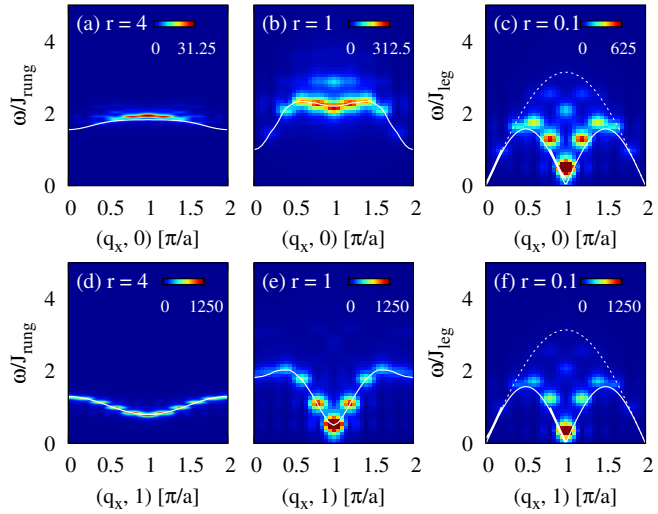

FIG. 8. The dynamical spin correlation function $S(\mathbf{q},\omega)$ evaluated for the undoped ladder with $r = \frac{J_{\rm rung}}{J_{\rm leg}} = \{4, 1, 0.1\}$ rung couplings, using ED and a 2×10 cluster. Panels (a)-(c) and (d)-(f) show the spectra along the $\mathbf{q} = (q_x, 0)$ and $\mathbf{q} = (q_x, \pi/a)$ directions, respectively. The overall intensity has been rescaled by a factor $1/\Gamma^2$, which corresponds to the prefactor relating $S(\mathbf{q},\omega)$ to the RIXS intensity. These plots capture all of the features of the spectra presented in Fig. 2.

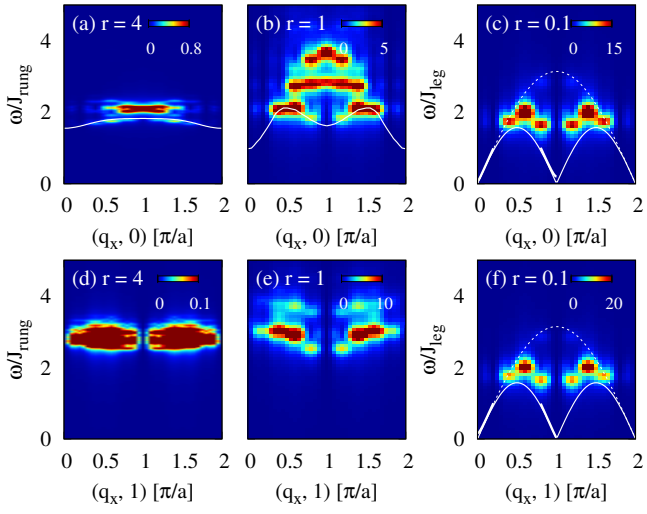

FIG. 9. The dynamical spin exchange correlation function $S^{\rm exch}(\mathbf{q},\omega)$ evaluated for the undoped ladder with $r = \frac{J_{\rm rung}}{J_{\rm leg}} = \{4, 1, 0.1\}$ rung couplings, using ED and a 2×10 cluster. Panels (a)-(c) and (d)-(f) show the spectra along the $\mathbf{q} = (q_x, 0)$ and $\mathbf{q} = (q_x, \pi/a)$ directions, respectively. The overall intensity was rescaled by a factor of $1/\Gamma^4$, which corresponds to the prefactor relating $S^{\rm exch}(\mathbf{q},\omega)$ to the RIXS intensity. These plots capture many of the features of the spectra Fig. 4.

Appendix A: Results for the dynamical correlation functions

The interpretation of RIXS spectra computed with the Kramers-Heisenberg formalism can be difficult. To simplify matters, the full RIXS intensity can be expanded in powers of J/Γ using the ultra-short core-hole lifetime (UCL) approximation. This procedure expresses the RIXS intensity as a series of increasingly complicated multi-particle correlation functions, which can then be further subdivided into correlation functions of the NSC and SC channels. The detailed procedure to be followed has been reported in several prior studies [68, 73, 77, 78]. Here, we evaluate some effective correlation functions motivated by Eqs. (B1) and (B2) of Ref. 68. In many cases, these simplified correlation functions give an accurate description of the RIXS intensity.

The spectral weight of the NSC channel is dominated by the first-order term in the UCL expansion, which is equivalent to the dynamical spin structure factor

$$S(\mathbf{q},\omega) = \frac{1}{L}\sum_f \left|\langle f|\sum_{i,\tau} e^{i\mathbf{q}\cdot\mathbf{R}_{i,\tau}} S^{\alpha}_{i,\tau}|g\rangle\right|^2 \delta(E_f - E_g + \omega). \tag{A1}$$

Here, S^{α}_i ($\alpha = \{\pm, z\}$) is the z component of the spin operator at site (i,τ). The $S(\mathbf{q},\omega)$ responses for an undoped ladder along the $(q_x, 0)$ and $(q_x, \pi/a)$ directions are plotted in Figs. 8(a)-(c) and 8(c)-(f), respectively. These results compare well with the RIXS intensity computed within the Kramers-Heisenberg formalism shown in Figs. 2 for all values of the rung coupling.

To account for the magnetic excitations of the SC channel, the second-order term in the UCL expansion of the Kramers-Heisenberg formula is needed [see Eq. (B2) of Ref. 68]. In the undoped case, the first-order term only contributes to the elastic line in this channel and a double spin-flip process appearing at second-order generates magnetic excitations. The RIXS spectra in the SC channel of the undoped ladders is hence dominated by the dynamical spin-exchange structure factor [68, 73, 74]

$$S^{\rm exch}(\mathbf{q},\omega) = \frac{1}{L}\sum_f \left|\langle f|\sum_{i,\tau} e^{i\mathbf{q}\cdot\mathbf{R}_{i,\tau}} O^{\rm exch}_{i,\tau}|g\rangle\right|^2 \times \delta(E_f - E_g + \omega). \tag{A2}$$

Here, $O^{\rm exch}_{i,\tau} = \mathbf{S}_{i,\tau}\cdot\left[J_{\rm leg}\left(\mathbf{S}_{i+1,\tau} + \mathbf{S}_{i-1,\tau}\right) + J_{\rm rung}\mathbf{S}_{i,\bar{\tau}}\right]/2$ evaluates the spin exchange between nearest-neighbor sites of the ladder, as sketched in Fig. 1(c) and 1(d).

The results for $S^{\rm exch}(\mathbf{q},\omega)$ in the undoped ladder along the $(q_x, 0)$ and $(q_x, \pi/a)$ directions are shown in Figs. 9(a)-(c) and 9(d)-(f), respectively. These results compare well with the RIXS intensities shown in Fig. 4 evaluted using the full Kramers-Heisenberg formalism. $S^{\rm exch}(\mathbf{q},\omega)$ captures the correct excitations for weak-rung couplings, but the intensities are overpredicted for strong-rung couplings, the regime where the UCL approximation is expected to fail (large J/Γ).

The SC channel for the doped ladders is dominated by charge excitations. In this case, one must also go to second order and the RIXS intensity is well approximated

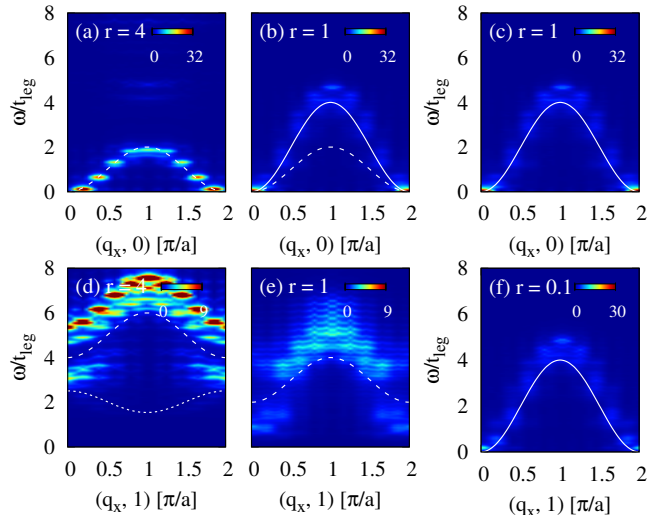

FIG. 10. The modified dynamical charge structure factor $\tilde{N}(\mathbf{q},\omega)$ evaluated for the doped ladder with $r = \frac{J_{\rm rung}}{J_{\rm leg}} = \{4, 1, 0.1\}$ rung couplings, using ED, a 2×10 cluster, and $n = 0.9$. Panels (a)-(c) and (d)-(f) show the spectra along the $\mathbf{q} = (q_x, 0)$ and $\mathbf{q} = (q_x, \pi/a)$ directions, respectively. The overall intensity has been rescaled by a factor $1/\Gamma^2$, corresponding to the prefactor relating $\tilde{N}(\mathbf{q},\omega)$ to the RIXS intensity. These plots capture many of the features of the spectra presented in Fig. 5.

by a modified dynamical charge structure factor [68]

$$\tilde{N}(q,\omega) = \frac{1}{L}\Big(\sum_f \Big|\langle f|\sum_{i,\tau} e^{i\mathbf{q}\cdot\mathbf{R}_{i,\tau}} O^1_{i,\tau}|g\rangle\Big|^2 + \frac{1}{\Gamma^2}\Big|\langle f|\sum_{i,\tau} e^{i\mathbf{q}\cdot\mathbf{R}_{i,\tau}} O^2_{i,\tau}|g\rangle\Big|^2\Big) \times \delta(E_f - E_g - \omega). \tag{A3}$$

Here, $O^1_{i,\tau} = \sum_\sigma c^\dagger_{i,\tau,\sigma} c_{i,\tau,\sigma}$, $O^2_{i,\tau} = \sum_\sigma [t_{\rm leg}(c^\dagger_{i+1,\tau,\sigma} + c^\dagger_{i-1,\tau,\sigma}) + t_{\rm rung} c^\dagger_{i,\bar{\tau},\sigma}] c_{i,\tau,\sigma}/2$, and $c_{i,\tau,\sigma}$ annihilates a spin σ hole at site (i,τ), subject to the constraint of no double occupancy. Results for $\tilde{N}(\mathbf{q},\omega)$ along the $(q_x, 0)$ and $(q_x, \pi/a)$ directions are shown in panels Fig. 10(a)-(c) and Fig. 10(d)-(f), respectively. In the doped case, the first-order term is non-zero but the majority of the intensity is set by the second-order term. The $\tilde{N}(\mathbf{q},\omega)$ results compare reasonably well to the RIXS spectra shown in Fig. 5 evaluated using the full Kramers-Heisenberg formalism.

Appendix B: X-ray absorption

For all the RIXS figures discussed in the main text, we tuned the incident photon energy to the peak position observed in the x-ray absorption (XAS) spectra given by

$$I(\omega_{\rm in}) = \sum_n \big|\langle n|D_{\mathbf{k}=0}|g\rangle\big|^2 \delta(E_n - E_g - \omega_{\rm in}). \tag{B1}$$

Figure 11 shows the XAS spectra for the undoped and doped cases as a function of the rung coupling

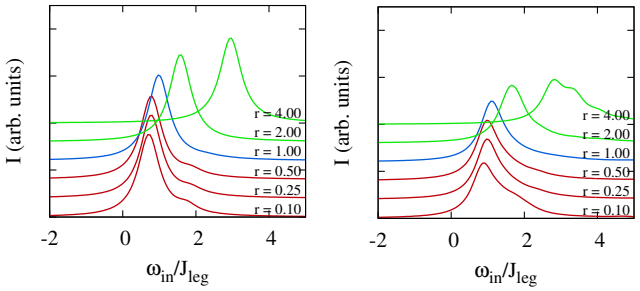

FIG. 11. XAS spectra for the undoped (left panel; $n = 1.0$) and doped (right panel; $n = 0.9$) ladders for various values of $r = \frac{J_{\rm rung}}{J_{\rm leg}}$, using ED and a 2×10 cluster. Increasing the rung coupling factor r, the peak position of the XAS shifts to higher incident photon energies.

$r = J_{\rm rung}/J_{\rm leg}$. For the undoped two-leg ladder, the resonance peak in the XAS spectra shifts to larger values of $\omega_{\rm in}$ with increasing rung coupling. In the strong-rung case ($r > 1$), the ladder acts as a collection of rung-dimers and the shift in the XAS peak reflects the increased cost of breaking the dimer singlets. For the doped two-leg ladder, the overall intensity of the XAS also decreases with increasing r while new peaks appear on the high-energy side of the resonance.

[1] E. Dagotto and T. M. Rice, Science **271**, 618 (1996).
[2] B. Lake, A. M. Tsvelik, S. Notbohm, D. Alan Tennant, T. G. Perring, M. Reehuis, C. Sekar, G. Krabbes, and B. Büchner, Nature Physics **6**, 50 (2009).
[3] J. Schlappa, K. Wohlfeld, K. J. Zhou, M. Mourigal, M. W. Haverkort, V. N. Strocov, L. Hozoi, C. Monney, S. Nishimoto, S. Singh, A. Revcolevschi, J.-S. Caux, L. Patthey, H. M. Rønnow, J. van den Brink, and T. Schmitt, Nature **485**, 82 (2012).
[4] J. Schlappa, U. Kumar, K. J. Zhou, S. Singh, M. Mourigal, V. N. Strocov, A. Revcolevschi, L. Patthey, H. M. Rønnow, S. Johnston, and T. Schmitt, Nature Communications **9**, 5394 (2018).
[5] J. Schlappa, T. Schmitt, F. Vernay, V. N. Strocov, V. Ilakovac, B. Thielemann, H. M. Rønnow, S. Vanishri, A. Piazzalunga, X. Wang, L. Braicovich, G. Ghiringhelli, C. Marin, J. Mesot, B. Delley, and L. Patthey, Phys. Rev. Lett. **103**, 047401 (2009).
[6] M. Mourigal, M. Enderle, A. Klöpperpieper, J.-S. Caux, A. Stunault, and H. M. Rønnow, Nature Physics **9**, 435 (2013).
[7] S. R. White and D. J. Scalapino, Phys. Rev. Lett. **91**, 136403 (2003).
[8] T. Nagao and J.-i. Igarashi, Phys. Rev. B **85**, 224436

(2012).
[9] D. Schmidiger, P. Bouillot, S. Mühlbauer, S. Gvasaliya, C. Kollath, T. Giamarchi, and A. Zheludev, Phys. Rev. Lett. **108**, 167201 (2012).
[10] M. Jeong, H. Mayaffre, C. Berthier, D. Schmidiger, A. Zheludev, and M. Horvatić, Phys. Rev. Lett. **118**, 167206 (2017).
[11] D. Schmidiger, S. Mühlbauer, A. Zheludev, P. Bouillot, T. Giamarchi, C. Kollath, G. Ehlers, and A. M. Tsvelik, Phys. Rev. B **88**, 094411 (2013).
[12] B. Thielemann, C. Rüegg, H. M. Rønnow, A. M. Läuchli, J.-S. Caux, B. Normand, D. Biner, K. W. Krämer, H.-U. Güdel, J. Stahn, K. Habicht, K. Kiefer, M. Boehm, D. F. McMorrow, and J. Mesot, Phys. Rev. Lett. **102**, 107204 (2009).
[13] R. S. Eccleston, M. Uehara, J. Akimitsu, H. Eisaki, N. Motoyama, and S.-i. Uchida, Phys. Rev. Lett. **81**, 1702 (1998).
[14] M. Matsuda, K. Katsumata, R. S. Eccleston, S. Brehmer, and H.-J. Mikeska, Phys. Rev. B **62**, 8903 (2000).
[15] J. E. Lorenzo, L. P. Regnault, C. Boullier, N. Martin, A. H. Moudden, S. Vanishri, C. Marin, and A. Revcolevschi, Phys. Rev. Lett. **105**, 097202 (2010).
[16] G. Deng, N. Tsyrulin, P. Bourges, D. Lamago, H. Ronnow, M. Kenzelmann, S. Danilkin, E. Pomjakushina, and K. Conder, Phys. Rev. B **88**, 014504 (2013).
[17] A. T. Savici, G. E. Granroth, C. L. Broholm, D. M. Pajerowski, C. M. Brown, D. R. Talham, M. W. Meisel, K. P. Schmidt, G. S. Uhrig, and S. E. Nagler, Phys. Rev. B **80**, 094411 (2009).
[18] J. E. Lorenzo, L. P. Regnault, C. Boullier, N. Martin, S. Vanishri, and C. Marin, Phys. Rev. B **83**, 140413 (2011).
[19] T. Hong, K. P. Schmidt, K. Coester, F. F. Awwadi, M. M. Turnbull, Y. Qiu, J. A. Rodriguez-Rivera, M. Zhu, X. Ke, C. P. Aoyama, Y. Takano, H. Cao, W. Tian, J. Ma, R. Custelcean, H. D. Zhou, and M. Matsuda, Phys. Rev. B **89**, 174432 (2014).
[20] A. Nocera, Y. Wang, N. D. Patel, G. Alvarez, T. A. Maier, E. Dagotto, and S. Johnston, Phys. Rev. B **97**, 195156 (2018).
[21] M. Uehara, T. Nagata, J. Akimitsu, H. Takahashi, N. Mri, and K. Kinoshita, Journal of the Physical Society of Japan **65**, 2764 (1996).
[22] E. Dagotto, J. Riera, and D. Scalapino, Phys. Rev. B **45**, 5744 (1992).
[23] S. Notbohm, P. Ribeiro, B. Lake, D. A. Tennant, K. P. Schmidt, G. S. Uhrig, C. Hess, R. Klingeler, G. Behr, B. Büchner, M. Reehuis, R. I. Bewley, C. D. Frost, P. Manuel, and R. S. Eccleston, Phys. Rev. Lett. **98**, 027403 (2007).
[24] L. Braicovich, J. van den Brink, V. Bisogni, M. M. Sala, L. J. P. Ament, N. B. Brookes, G. M. De Luca, M. Salluzzo, T. Schmitt, V. N. Strocov, and G. Ghiringhelli, Phys. Rev. Lett. **104**, 077002 (2010).
[25] V. Bisogni, L. Simonelli, L. J. P. Ament, F. Forte, M. Moretti Sala, M. Minola, S. Huotari, J. van den Brink, G. Ghiringhelli, N. B. Brookes, and L. Braicovich, Phys. Rev. B **85**, 214527 (2012).
[26] M. Le Tacon, M. Minola, D. C. Peets, M. Moretti Sala, S. Blanco-Canosa, V. Hinkov, R. Liang, D. A. Bonn, W. N. Hardy, C. T. Lin, T. Schmitt, L. Braicovich, G. Ghiringhelli, and B. Keimer, Phys. Rev. B **88**, 020501 (2013).
[27] M. Minola, G. Dellea, H. Gretarsson, Y. Y. Peng, Y. Lu, J. Porras, T. Loew, F. Yakhou, N. B. Brookes, Y. B. Huang, J. Pelliciari, T. Schmitt, G. Ghiringhelli, B. Keimer, L. Braicovich, and M. Le Tacon, Phys. Rev. Lett. **114**, 217003 (2015).
[28] H. Y. Huang, C. J. Jia, Z. Y. Chen, K. Wohlfeld, B. Moritz, T. P. Devereaux, W. B. Wu, J. Okamoto, W. S. Lee, M. Hashimoto, Y. He, Z. X. Shen, Y. Yoshida, H. Eisaki, C. Y. Mou, C. T. Chen, and D. J. Huang, Scientific Reports **6**, 19657 (2016).
[29] M. Le Tacon, G. Ghiringhelli, J. Chaloupka, M. M. Sala, V. Hinkov, M. W. Haverkort, M. Minola, M. Bakr, K. J. Zhou, S. Blanco-Canosa, C. Monney, Y. T. Song, G. L. Sun, C. T. Lin, G. M. De Luca, M. Salluzzo, G. Khaliullin, T. Schmitt, L. Braicovich, and B. Keimer, Nature Physics **7**, 725 (2011).
[30] W. S. Lee, J. J. Lee, E. A. Nowadnick, S. Gerber, W. Tabis, S. W. Huang, V. N. Strocov, E. M. Motoyama, G. Yu, B. Moritz, H. Y. Huang, R. P. Wang, Y. B. Huang, W. B. Wu, C. T. Chen, D. J. Huang, M. Greven, T. Schmitt, Z. X. Shen, and T. P. Devereaux, Nature Physics **10**, 883 (2014).
[31] L. J. P. Ament, G. Ghiringhelli, M. M. Sala, L. Braicovich, and J. van den Brink, Phys. Rev. Lett. **103**, 117003 (2009).
[32] X. Lu, P. Olalde-Velasco, Y. Huang, V. Bisogni, J. Pelliciari, S. Fatale, M. Dantz, J. G. Vale, E. C. Hunter, J. Chang, V. N. Strocov, R. S. Perry, M. Grioni, D. F. McMorrow, H. M. Rønnow, and T. Schmitt, Phys. Rev. B **97**, 041102 (2018).
[33] V. Bisogni, M. Moretti Sala, A. Bendounan, N. B. Brookes, G. Ghiringhelli, and L. Braicovich, Phys. Rev. B **85**, 214528 (2012).
[34] F. Forte, M. Cuoco, C. Noce, and J. van den Brink, Phys. Rev. B **83**, 245133 (2011).
[35] S. Kourtis, J. van den Brink, and M. Daghofer, Phys. Rev. B **85**, 064423 (2012).
[36] U. Kumar, A. Nocera, E. Dagotto, and S. Johnston, New Journal of Physics **20**, 073019 (2018).
[37] C. J. Jia, E. A. Nowadnick, K. Wohlfeld, Y. F. Kung, C.-C. Chen, S. Johnston, T. Tohyama, B. Moritz, and T. P. Devereaux, Nature Communications **5**, 3314 (2014).
[38] A. Higashiya, S. Imada, T. Murakawa, H. Fujiwara, S. Kasai, A. Sekiyama, S. Suga, K. Okada, M. Yabashi, K. Tamasaku, T. Ishikawa, and H. Eisaki, New Journal of Physics **10**, 053033 (2008).
[39] L. Wray, D. Qian, D. Hsieh, Y. Xia, H. Eisaki, and M. Z. Hasan, Phys. Rev. B **76**, 100507 (2007).
[40] K. Ishii, K. Tsutsui, T. Tohyama, T. Inami, J. Mizuki, Y. Murakami, Y. Endoh, S. Maekawa, K. Kudo, Y. Koike, and K. Kumagai, Phys. Rev. B **76**, 045124 (2007).
[41] V. Bisogni, S. Kourtis, C. Monney, K. Zhou, R. Kraus, C. Sekar, V. Strocov, B. Büchner, J. van den Brink, L. Braicovich, T. Schmitt, M. Daghofer, and J. Geck, Phys. Rev. Lett. **112**, 147401 (2014).
[42] V. Bisogni, K. Wohlfeld, S. Nishimoto, C. Monney, J. Trinckauf, K. Zhou, R. Kraus, K. Koepernik, C. Sekar, V. Strocov, B. Büchner, T. Schmitt, J. van den Brink, and J. Geck, Phys. Rev. Lett. **114**, 096402 (2015).
[43] A. Nocera, U. Kumar, N. Kaushal, G. Alvarez, E. Dagotto, and S. Johnston, Scientific Reports **8**, 11080 (2018).
[44] S. R. White, Phys. Rev. Lett. **69**, 2863 (1992).

[45] S. R. White, Phys. Rev. B **48**, 10345 (1993).

[46] B. J. Kim, H. Jin, S. J. Moon, J.-Y. Kim, B.-G. Park, C. S. Leem, J. Yu, T. W. Noh, C. Kim, S.-J. Oh, J.-H. Park, V. Durairaj, G. Cao, and E. Rotenberg, Phys. Rev. Lett. **101**, 076402 (2008).

[47] L. J. P. Ament, G. Khaliullin, and J. van den Brink, Phys. Rev. B **84**, 020403 (2011).

[48] J. Kim, D. Casa, M. H. Upton, T. Gog, Y.-J. Kim, J. F. Mitchell, M. van Veenendaal, M. Daghofer, J. van den Brink, G. Khaliullin, and B. J. Kim, Phys. Rev. Lett. **108**, 177003 (2012).

[49] H. Gretarsson, N. H. Sung, J. Porras, J. Bertinshaw, C. Dietl, J. A. N. Bruin, A. F. Bangura, Y. K. Kim, R. Dinnebier, J. Kim, A. Al-Zein, M. Moretti Sala, M. Krisch, M. Le Tacon, B. Keimer, and B. J. Kim, Phys. Rev. Lett. **117**, 107001 (2016).

[50] J. H. Gruenewald, J. Kim, H. S. Kim, J. M. Johnson, J. Hwang, M. Souri, J. Terzic, S. H. Chang, A. Said, J. W. Brill, G. Cao, H.-Y. Kee, and S. S. A. Seo, Advanced Materials **29**, 1603798 (2017).

[51] A. Gozar, G. Blumberg, B. S. Dennis, B. S. Shastry, N. Motoyama, H. Eisaki, and S. Uchida, Phys. Rev. Lett. **87**, 197202 (2001).

[52] L. J. P. Ament, M. van Veenendaal, T. P. Devereaux, J. P. Hill, and J. van den Brink, Rev. Mod. Phys. **83**, 705 (2011).

[53] W. Zheng, C. J. Hamer, R. R. P. Singh, S. Trebst, and H. Monien, Phys. Rev. B **63**, 144410 (2001).

[54] K. P. Schmidt and G. S. Uhrig, Phys. Rev. Lett. **90**, 227204 (2003).

[55] K. P. Schmidt and G. S. Uhrig, Modern Physics Letters B **19**, 1179 (2005).

[56] T. Barnes, E. Dagotto, J. Riera, and E. S. Swanson, Phys. Rev. B **47**, 3196 (1993).

[57] The triplon and bound two-triplon excitations are often referred to as magnon and bound two-magnon excitations, respectively, in the literature. We have adopted the triplon nomenclature to be consistent with the previous RIXS studies [5, 8].

[58] Knetter, C., Schmidt, K. P., and Uhrig, G. S., Eur. Phys. J. B **36**, 525 (2003).

[59] O. P. Sushkov and V. N. Kotov, Phys. Rev. Lett. **81**, 1941 (1998).

[60] M. Greven, R. J. Birgeneau, and U. J. Wiese, Phys. Rev. Lett. **77**, 1865 (1996).

[61] D. G. Shelton, A. A. Nersesyan, and A. M. Tsvelik, Phys. Rev. B **53**, 8521 (1996).

[62] M. Troyer, H. Tsunetsugu, and T. M. Rice, Phys. Rev. B **53**, 251 (1996).

[63] S. Liu, H.-C. Jiang, and T. P. Devereaux, Phys. Rev. B **94**, 155149 (2016).

[64] S. R. White, D. J. Scalapino, and S. A. Kivelson, Phys. Rev. Lett. **115**, 056401 (2015).

[65] N. J. Robinson, F. H. L. Essler, E. Jeckelmann, and A. M. Tsvelik, Phys. Rev. B **85**, 195103 (2012).

[66] A. Nocera, N. D. Patel, E. Dagotto, and G. Alvarez, Phys. Rev. B **96**, 205120 (2017).

[67] E. H. Lieb and F. Y. Wu, Phys. Rev. Lett. **20**, 1445 (1968).

[68] C. Jia, K. Wohlfeld, Y. Wang, B. Moritz, and T. P. Devereaux, Phys. Rev. X **6**, 021020 (2016).

[69] T. F. A. Müller and T. M. Rice, Phys. Rev. B **58**, 3425 (1998).

[70] T. Tohyama, M. Mori, and S. Sota, Phys. Rev. B **97**, 235137 (2018).

[71] J. M. Tranquada, H. Woo, T. G. Perring, H. Goka, G. D. Gu, G. Xu, M. Fujita, and K. Yamada, Nature **429**, 534 (2004).

[72] G. Xu, G. D. Gu, M. Hücker, B. Fauqué, T. G. Perring, L. P. Regnault, and J. M. Tranquada, Nature Physics **5**, 642 (2009).

[73] F. Forte, L. J. P. Ament, and J. van den Brink, Phys. Rev. B **77**, 134428 (2008).

[74] A. Klauser, J. Mossel, J.-S. Caux, and J. van den Brink, Phys. Rev. Lett. **106**, 157205 (2011).

[75] D. Benjamin, I. Klich, and E. Demler, Phys. Rev. Lett. **112**, 247002 (2014).

[76] M. Kanász-Nagy, Y. Shi, I. Klich, and E. A. Demler, Phys. Rev. B **94**, 165127 (2016).

[77] J. van den Brink and M. van Veenendaal, EPL (Europhysics Letters) **73**, 121 (2006).

[78] L. J. P. Ament, F. Forte, and J. van den Brink, Phys. Rev. B **75**, 115118 (2007).